Chapter 5

Probing the variations in the reversal timing of the Sun's polar field

5.1 Introduction

The strength of the large-scale magnetic field of the Sun oscillates while the polarity flips in about 11 years. Around the time of solar minimum, the magnetic field near the poles becomes maximum in its strength and then decreases with the progress of the solar cycle. Eventually, around the time of solar maximum, polar field reversal occurs. It is observed (and modelled by the surface flux transport (SFT) and dynamo models) that the decay and dispersals of the tilted Bipolar Magnetic Regions (BMRs) generates a poloidal magnetic field in low latitudes (Babcock, 1961b; Leighton, 1969). This field is transported towards the poles through meridional circulation and cancels the opposite polarity fields that exist around the poles. Thus, the properties of the BMRs (primarily the tilt, amount of flux and the rate of emergence) and the surface flows determine the growth rate and the time of reversal of the polar field (Baumann et al., 2004; Jiang et al., 2014a; Karak et al., 2018; Kumar et al., 2022; Mordvinov et al., 2022b).

The polar magnetic field is a good measure of the strength of the next solar cycle (Choudhuri et al., 2007b; Kumar et al., 2021; Makarov et al., 1989; Petrovay, 2020; Priyal et al., 2014; Schatten et al., 1978b). This is because the poloidal magnetic field is transported down to the deeper convection zone where the differential rotation stretches it to induce a toroidal magnetic field which is the seed for the sunspots of the next cycle (Charbonneau, 2020; Karak et al., 2014). If the polar field reverses early, then the next cycle begins early because the toroidal field and thus the sunspots for the next cycle will also emerge early. Furthermore, early polar field reversal will lead to early termination of the sunspot production and the ongoing cycle will reach to end early. This is because the early reversal will quickly annihilate the old polarity poloidal field, thereby stopping the generation of the toroidal field of the current cycle. Late polar reversal will cause the delayed end of the current cycle, resulting a strong asymmetry in its shape; the decline phase will be longer than the rising phase (Kitchatinov and Nepomnyashchikh, 2018). Moreover, a delayed polar field reversal will lead to the late beginning of the next solar cycle. Thus, in many ways, the timing of the reversals determines the length and shape of the current cycle and the beginning of the following cycle. Therefore, the analysis of regular long-term measurements of the magnetic field is one of the key points to understand the evolution of solar activity, to make its reliable predictions and to forecast the space weather and geomagnetic disturbances.

In the observations of the past few cycles, it has been found that the polar field reversal timing is not fixed (Golubeva et al., 2023). It varies by a few years from cycle to cycle with respect to the average interval of 11 years. Thus, polar field reversals have attracted special attention since their discovery (Babcock, 1959) and promotion to the forefront in simulations of cyclic MHD-processes in the heliosphere (Babcock, 1961b). A reversal of the solar poloidal field completes global restructuring in the heliospheric magnetic configuration. Besides, it anticipates the appearance of long-lived transequatorial coronal

holes, which are the main geoeffective phenomenon during solar activity minima (Petrie, 2015).

Hence, it becomes an important task to understand the primary reasons behind the delayed or early reversals of the Sun's polar field in different cycles. In this study, we employ the SFT simulations similar to the what has been described in Chapter 4 with variations in the properties of BMRs and with the inclusion of anomalous BMRs to probe the variations in the polar field reversal timing.

5.2 Observational results

Before I jump into discussing the simulation setup, let me briefly mention the observational findings as reported in Golubeva et al. (2023) which works as the motivation behind performing simulations to be discussed in the later parts of the chapter. Golubeva et al. (2023) analyzed the magnetographic observations of the Sun's photospheric magnetic field from different space and ground-based observatories namely MWO/STT, SoHO/MDI, SOLIS/VSM, SDO/HMI for Cycles 21-24. The polar field is calculated from a latitudinal band $\pm(65^\circ - 80^\circ)$ in the northern and southern hemispheres. The data is corrected for the zero-field offset of the magnetograms near the polar caps and it is further smoothed with a moving averaging window of 13 CR (Carrington Rotation) to avoid fluctuations in the measurements. For further details regarding the approach of data analysis, the reader is referred to sections 3-5 of Golubeva et al. (2023). The final measurement of the polar field reversal timing from the peak of the polar field (or near the minima of the solar cycle) in terms of the Carrington Rotation is presented in the Table 5.1. The final column of the table provides the reversal timing (T_r) of the hemispheric polar field for different cycles. It is pretty much evident that the polar field reversal timing has shown significant variations in different cycles, where Cycle 22 exhibited an early reversal of the polar field and on the other hand Cycle 24 showed a much delayed polar field reversal.

Table 5.1 Analysis of the timing of hemispheric North/South (N/S) polar field reversal timing (T_r) as observed from different observatories and reported in Table-3 of Golubeva et al. (2023). The T_r is calculated from the difference between the Carrington Rotation number between the start of the cycle and during the reversal of the polar field as measured between the latitudinal band of $\pm(65^\circ - 80^\circ)$. The zero crossing time (in terms of CR) of the polar field in three hemispheric latitudinal bands with a width of 5° is also mentioned in the column 6-8.

Data origin	Cycle	Start, CR*	Maximum, CR(N/S)*	Zero crossing time, CR				T_r, CR(N/S)
				Latitude				
				N/S (65 – 80)°	N/S 67.5°	N/S 72.5°	N/S 77.5°	
Primordial data after the noise correction								
MWO/STT	21	1639	1686/1694	1692/1700	1690/1696	1693/1701	1694/1708	53/61
–	22	1779	1820/1844	1825/1842	1820 – 21/1840	1825/1843	1828/1844	46/63
–	23	1913	1965/1986	1959/1968	1956/1963	1960/1969	1964 – 65/1973	46/55
SoHO/MDI	–	–	–	1966/1973	- /1970	1972/1975	- / -	53/60
SOLIS/VSM	24	2078	2119/2147	2132/2148	2126 – 27/2141	2133/2148	2136/2154 – 55	54/70
SDO/HMI	–	–	–	2132/2149	- /2142	- /2151	2136/2155 – 56	54/71
Data corrected for the noise and for zero-level offset								
MWO/STT	21	1639	1686/1694	1695/1695	1691/1692	1695/1696	1697/1704	56/56
–	22	1779	1820/1844	1828/1828	1821/1824	1827/1829	1832/1830 – 31	49/49
–	23	1913	1965/1986	1964 – 65/1966	1957/1956 – 57	1963/1966	1967/1970 – 71	51 – 52/53
SoHO/MDI	–	–	–	1962/1975	- /1972	1968/1976	- / -	49/62
SOLIS/VSM	24	2078	2119/2147	2137/2152 – 53	2130/2142	2137/2150	2139/2164 – 65	61/74 – 75
SDO/HMI	–	–	–	2135/2151	- /2139 – 40	2138/2149 – 50	2135 – 36/2158 – 59	57/73

* According to Monthly Hemispheric Sunspot Data from https://www.sidc.be/silso/extheminum

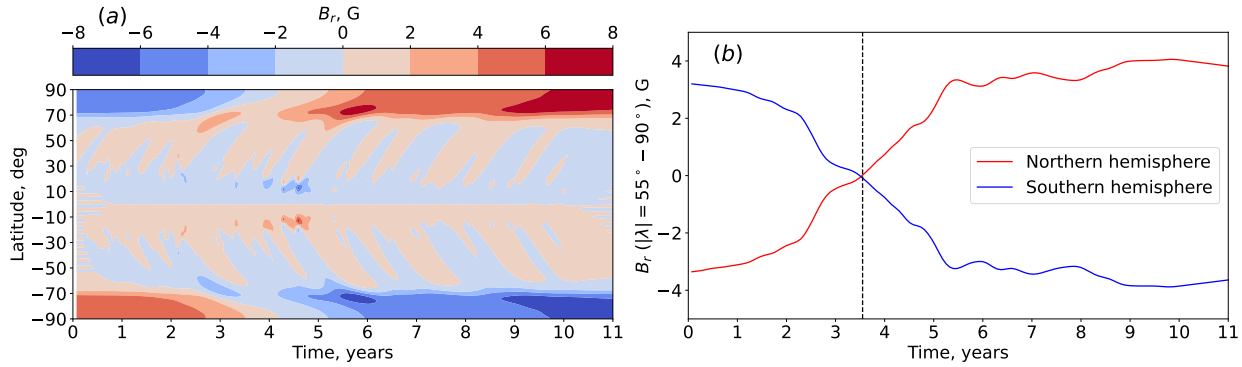

Fig. 5.1 Evolution of the radial surface field (a) and the corresponding evolution of the polar fields (b) from one of the simulations. The dashed vertical line in the panel (b) represents the reversal time T_r. Image Credit: Golubeva et al. (2023)

5.3 Results from the Surface Flux Transport simulations

Here in this section, I would like to emphasize the properties of the evolution of BMRs that determine the reversals in the polar fields and their eventual build-up. For this purpose, we are utilizing the SFT model. The SFT model captures the essence of the so-called Babcock-Leighton (B-L) mechanism for the decay and dispersal of the tilted BMRs and the subsequent poleward motion of the remaining radial field under the influence of meridional circulation, differential rotation and horizontal diffusion (Baumann et al., 2004; Sheeley et al., 1985; Wang and Sheeley, 1989). In the previous chapter, an elaborate discussion about the SFT simulations has been presented.

The various properties of the BMRs especially the distribution of the BMR tilt vary widely from one cycle to another and it is thought to be the primary reason for the wide range of variability in the long term modulation of the solar cycles (Biswas et al., 2023b; Karak and Miesch, 2017; Karak, 2023; Lemerle and Charbonneau, 2017). The tilt of the BMRs increases with the increase in the emergence latitude according to the formula known as the Joy's law (Hale et al., 1919). However it has been observed that, although the tilts obey the Joy's law statistically, they exhibit a huge scatter (Fisher et al. (1995); Howard (1991); Jha et al. (2020), also see Fig. 4 of Karak (2023)). Due to this scatter in

the BMR tilts, the contribution of different BMRs in the ultimate build-up of the polar field vary widely (Jiang et al., 2014a; Karak and Miesch, 2018). Often, the tilts and the orientation of magnetic polarities of certain BMRs are opposite to that of the regular BMRs, as a result, they contribute negatively in the polar field build-up. In certain cases, they can produce large fluctuations in the polar field leading to extreme events like the Maunder Minimum (Nagy et al., 2017). These kinds of BMRs are known as the 'anomalous' or 'rogue' BMRs (such as anti-Joy or anti-Hale BMRs). It is obvious that the presence of these anomalous BMRs will have an impact on the amplitude and reversal time of the polar field. However, there is a lack of understanding regarding how the polar field reversal time is affected due to the presence of these BMRs in different phases of the solar cycles, and there has been very few studies in the past attempting to qauntify their impact on reversal timing (see for example, Nagy et al. (2017); Pal et al. (2023)). Pal et al. (2023) included anomalous regions in varied amounts and with spatio-temporal variations (having flux content of 5% and 10% of the total flux), claiming that the anti-Hale and anti-Joy regions impact the evolution of the polar field in a similar manner, however they did not include the significant observed scatter in BMR tilts around Joy's law (for example, see Fig. 4 of Karak, 2023) in their study. Here we utilize the aforementioned SFT simulations to take a look at how the variation in the BMR tilt properties and the inclusion of the anomalous BMRs (anti-Joy and anti-Hale) in different phases of the solar cycles impact the timing of the polar field reversal. Here we would like to mention that, in this study, we refer the BMRs as the active-regions that tightly correlate with the solar cycle and strictly follow the time-latitude trend of the butterfly diagram. The ephemeral regions that do not tighly follow the solar cycle and have large scatter in their tilts (Hagenaar et al., 2003; Sreedevi et al., 2024) are not included in our simulations.

To produce the synthetic spatiotemporal profiles of the BMRs that closely resembles the observed properties, we follow the analytical prescriptions as provided in Hathaway et al. (1994a) and Jiang et al. (2018).

For the tilt of the BMRs, we introduce a Gaussian scatter around the value of tilt obtained from the Joy's law: $\gamma = \gamma_0 \sin\lambda$,with $\gamma_0 = 35^\circ$ (Hale et al., 1919; Howard, 1991; Wang and Sheeley, 1989). The tilts of the anti-Joy BMRs are within the range of $-90^\circ < \gamma < 0^\circ$ whereas the tilts of the anti-Hale BMRs for which the conventional longitudinal orientation of the BMR polarities are flipped, falls within the range of $-180^\circ < \gamma < -90^\circ$. For our study, we allocate the amount of these anomalous BMRs randomly for different cycles. The percentage of the anti-Joy BMRs have taken to be within the range of $10-30\%$ whereas the percentage of the anti-Hale BMRs have taken within the range of $3-7\%$ keeping consistent with the observations (McClintock et al., 2014). These synthetic BMRs are the inputs to the SFT code for studying the evolution of the polar field. The profile of the solar cycles and the BMR properties are similar to the ones presented in the Chapter 4.

To compute the strength of the polar field from the simulations, we produce magnetogram maps at each 27 days interval (period of the Bartels Rotation, i.e. the rotation period of Sun near the equator in our model). From these maps the longitudinal averages of the surface magnetic fields are taken which provides the latitudinal migration of the fields with time. In the next step, the average value of the radial surface magnetic field from 55° to 90° latitudes is taken to be the polar field strength in each of these maps. The evolution of the surface radial field is shown in the panel (a) of Figure 5.1 whereas, the evolution of the corresponding polar field is presented in the panel (b), the vertical black dashed line shows the time of the reversal (T_r) of the polar field.

In this study, we present five different cases with different properties of the tilt of the BMRs. Here a list of these cases are given below:

(i) Cycles with all the BMR tilts obtained from the Joy's law.

(ii) Cycles with variation in the BMR tilt properties (i.e. having anti-Joy BMRs), without any anti-Hale BMRs present in the cycles.

(iii) Cycles with variation in the BMR tilt properties and anti-Hale BMRs present throughout all the phases of the cycles.

(iv) Cycles with variation in the BMR tilt properties and anti-Hale BMRs being present only in the rising phases of the cycles.

(v) Cycles with variation in the BMR tilt properties and anti-Hale BMRs being present only in the declining phases of the cycles.

Here we mention that for the analysis of the reversal time of polar field, 30 cycles has been simulated for each of these cases. The amplitudes of the simulated solar cycles vary within a range of 30 to 90 in terms of monthly BMR number. In the cycles for the Cases (ii), (iii), (iv) and (v), the anti-Joy BMRs are present randomly throughout the cycles, whereas, the presence of the anti-Hale BMRs, in the last three cases, are varied in the different phases of the cycles as mentioned earlier.

Finally, in the Table 5.2, we summarize the statistics of the timings of the polar field reversals for each of the above mentioned cases. The values of the average reversal times of the polar field for different cases matches well with the results obtained from the observations as noted in the last column of Table 5.1. From the Table 5.2, it can be clearly seen that the presence of the 'anomalous' BMRs in different phases of the cycles significantly impacts the reversal time. As in the Case (i) the tilts of the BMRs strictly follow the Joy's law, there are no 'anomalous' regions present in this case. Hence the reversal time is the shortest for these cycles. Comparing the Case (i) with the Case (ii), we can infer that the anti-Joy regions present in the cycles of the Case (ii) imposes only a slight delay in the reversal time. However, when the cycles of Case (iii) consists of some anti-Hale regions along with the anti-Joy regions, it produces a significant amount

of delay in the reversal time. On the other hand, when the cycles of Case (iv) consists of large amounts of anti-Hale regions concentrated in their initial phases, the delay is further enhanced to a large extent. The rising phases of the cycles in Case (v) are very similar to those of the cycles in Case (ii), i.e. the cycles from both the cases has only anti-Joy BMRs in their initial phases. Hence, their reversals time also have similar values. However, it is worth mentioning that, on an average, the cycles of Case (v) take slightly more time for their polar field reversal than the cycles of Case (ii). This is due to the presence of significant amount of anti-Hale BMRs during the maxima phases of the cycles, which have caused significant delay in polar field reversal for few cycles of Case (v), making the average value of reversal time for this case to be slightly higher.

In this study, we have explored the possible cases for the presence of the anti-Hale regions keeping their amount to be within a range of 3-7% for different cycles. As a result, when we spread them out throughout the cycle (Case (iii)), their temporal density is less compared to the case when they are present in a certain phase of the cycle (e.g., Case (iv)). We emphasize that, the significant delay in the polar field reversal can be caused due to an enhanced temporal density of anti-Hale BMRs in the beginning phases of the cycles as seen in Case (iv). However, when the temporal density of the anti-Hale BMRs for Case (iv) is kept similar to the Case (iii) by lowering their percentage amount, we would get a value of the reversal time similar to that of Case (iii).

The results discussed above regarding the impact of anomalous regions on the polar field reversal time are in qualitative agreement with Nagy et al. (2017) and Pal et al. (2023). However, these results indicate that, the anti-Hale regions are a much greater source of disturbance in the evolution of the polar field than the anti-Joy regions. The simulation results of Table 5.2 further hint towards the possibility that the significant scatter in the observed values of T_r for different cycles as presented in Table 5.1 may have been caused

Table 5.2 The mean of the reversal time ($< T_r >$) and their corresponding standard deviation (σ_{T_r}) from the simulations of 30 cycles belonging to each of the cases mentioned above (as presented in Table-4 of Golubeva et al. (2023)). The unit of the quantities are presented in terms of years as well as in CRs.

Case	$< T_r >$ Years (CRs)	σ_{T_r} Years (CRs)
(i)	3.59 (48.07)	1.08 (14.46)
(ii)	3.67 (49.14)	0.89 (11.92)
(iii)	3.85 (51.56)	1.11 (14.86)
(iv)	4.19 (56.11)	0.96 (12.85)
(v)	3.69 (49.41)	1.11 (14.86)

due to the presence of anti-Hale and anti-Joy regions in varied amount throughout the different phases of the solar Cycles 21 – 24.

5.4 Conclusion

We performed SFT simulations, to probe the origin of the observed significant cycle-to-cycle variations in the polar field reversal time. We found that the variation in the tilt properties of BMRs and the presence of 'anomalous' BMRs in different phases of the cycles impacts the polar field reversal time significantly. The presence of 'anomalous' regions in the early phases of the cycles imparts a considerable delay in the reversal time. We also find the impact of anti-Hale regions on the reversal time to be more pronounced than the anti-Joy type BMRs.